Nanoscale

PAPER

View Article Online
View Journal | View Issue

Cite this: *Nanoscale*, 2025, **17**, 15512

Mechanistic investigation of calcium phosphate mineralization potentiating the cellular immune response of foot-and-mouth disease virus-like particle vaccines†

Zhidong Teng,‡[a] Jiajun Li,‡[a] Mei Ren,[a] Qianqian Xie,[a] Hu Dong,[a] Jingjing Zhou,[a] Suyu Mu,[a] Manyuan Bai,[a] Shiqi Sun*[a] and Huichen Guo *[a,b,c]

Virus-like particles (VLPs), composed of structural proteins, have emerged as a promising vaccine platform for preventing infectious diseases due to their outstanding advantages. Enhancing immune responses specific to VLPs, particularly cellular immunity, has emerged as a pivotal area of current immunological research. The nanovaccines for the foot-and-mouth disease virus (FMDV) composed of VLPs mineralized with calcium phosphate (VLPs-CaP), developed based on biomineralization principles, demonstrates superior immunogenicity. In this study, we elucidated the efficacy and mechanism of VLPs-CaP in eliciting cellular immune responses. The results demonstrated that VLPs-CaP were efficiently internalized by dendritic cells (DCs) *via* energy-dependent endocytosis mediated by actin, microtubules, and clathrin. Upon uptake, VLPs-CaP decomposed within lysosomes, leading to the release of Ca^{2+} ions and an increase in lysosomal permeability. This facilitates the escape of VLPs into the cytoplasm for cross-presentation. Furthermore, CaP mineralization enhanced the level of activation of DCs by FMDV VLPs, evidenced by elevated expression of CD40 and CD86, and the secretion of IL-2 and IL-12p70. Immunization studies in mice revealed that VLPs-CaP elicited higher levels of specific antibodies compared to unmineralized VLPs; notably, there was an increased IgG2a/IgG1 ratio along with a greater number of cytotoxic T lymphocytes (CTLs). This study elucidated the mechanism by which CaP-mineralized VLPs induce cellular immune responses, offering new insights and strategies aimed at enhancing the cellular immune efficacy of VLP-based vaccines that primarily elicit humoral immunity.

Received 27th February 2025,
Accepted 22nd May 2025

DOI: 10.1039/d5nr00866b

rsc.li/nanoscale

Introduction

Infectious diseases impose a tremendous burden on global healthcare systems, as well as on social and economic facets. In the history of medicine, vaccination has proven to be the most successful and cost-efficient intervention measure. Virus-like particles (VLPs) present significant biomedical advantages: (1) inherent safety derived from the absence of viral genomes; (2) structural conformation preserving natural viral architecture with repetitive antigenic epitopes, enabling potent humoral and cellular immune activation; and (3) high modularity in targeted antigen display through bioengineering. These attributes have established VLPs as a robust vaccine platform, with licensed products demonstrating a favorable immunoprotective effect against hepatitis B virus, human papillomavirus, and hepatitis A/E viruses.[1–3]

VLPs have also attracted substantial attention in the research and development of veterinary vaccines. Foot-and-mouth disease (FMD) is a highly contagious viral disease in cloven-hoofed animals, which is widely prevalent across the globe and incurs severe economic losses. In FMD-endemic regions, vaccination serves as the principal approach for the prevention and control of FMD outbreaks. The VLPs in the vaccine for the FMDV, consisting of structural proteins, exhibit excellent safety and immunogenicity, and are regarded as components of an ideal candidate vaccine to replace inactivated vaccines and realize the eradication of FMD.[4,5] As exogenous antigens, VLPs mainly undergo presentation *via* MHC II molecules upon entry into antigen-presenting cells (APCs), which activates $CD4^+$ T lymphocytes and assists in inducing a favor-

[a]*State Key Laboratory for Animal Disease Control and Prevention, College of Veterinary Medicine, Lanzhou University, Lanzhou Veterinary Research Institute, Chinese Academy of Agricultural Sciences, Lanzhou, China.*
E-mail: guohuichen@caas.cn, shiqisun@caas.cn
[b]*College of Veterinary Medicine, Gansu Agricultural University, Lanzhou, China*
[c]*School of Life Sciences, Ningxia University, Yinchuan, China*
†Electronic supplementary information (ESI) available. See DOI: https://doi.org/10.1039/d5nr00866b
‡These authors contributed equally to this work.

able humoral immune response. However, their capacity to drive the cellular immune reaction is relatively weak.[6,7] Nevertheless, the vaccine's protective efficacy in combating pathogen infections is the synergistic result of both cellular immunity and humoral immunity.[8,9] Therefore, optimizing the cellular immune response elicited by VLPs in vaccines to attain superior immune protection has emerged as the focal point of current research.

With the rapid advancement of nanotechnology in the biological field, biomineralized nanovaccines have been extensively investigated.[10,11] These nanovaccines feature accurate regulation of physicochemical properties, pH responsiveness, and the ability to efficiently recruit and activate APCs.[12–14] Recent studies have shown that mineralized nanovaccines can elicit distinct immune responses by activating the innate immune system through two pathways after being taken up by APCs: (1) antigens are degraded within lysosomes and presented to $CD4^+$ T cells *via* MHC II, which assist in the differentiation of B lymphocytes into plasma cells, leading to the secretion of specific antibodies; (2) the mineralized layer rapidly disintegrates within the lysosomes, thereby disrupting the integrity of the lysosomal membrane and allowing antigens to escape into the cytoplasm. These antigens are then presented to $CD8^+$ T cells *via* MHC I, inducing the cellular immune response.[15–17] As exemplified by metal–organic framework (MOF)-mineralized ovalbumin (OVA) nanocomposites and silica-encapsulated VLP formulations targeting hepatitis B virus (HBV) and human papillomavirus (HPV), these advanced vaccine platforms demonstrate comparable lysosomal escape capabilities coupled with synergistic activation of both cellular and humoral immune responses.[6,18] Calcium phosphate (CaP), known for its excellent biocompatibility and ability to enhance immune responses, has been utilized as an adjuvant in various vaccines. In recognition of its safety and effectiveness, the World Health Organization has approved its use in human vaccines.[19,20] CaP achieves this enhancement through multiple pathways, including the depot effect, which prolongs the release of antigens, activation of the NLRP3 inflammasome to promote the secretion of inflammatory cytokines, and increased antigen uptake by APCs.[21–23] VLPs possess a controllable three-dimensional structure with multiple functional groups on their surface. The abundance of negatively charged amino acid residues enables VLPs to bind with Ca^{2+}, forming a CaP mineralization layer in the presence of PO_4^{3-}.[15] To date, no study explicitly elucidates the orientation and specific mechanisms of immune responses induced by CaP-mineralized FMDV VLPs.

In this study, by utilizing the ability of Ca^{2+} to bind with carboxyl, hydroxyl, and carbonyl groups present on protein surfaces,[15] FMDV VLPs-CaP nanoparticles were prepared by optimizing the mineralization conditions based on previous studies.[16] Our findings demonstrated that VLPs-CaP were taken up by DCs *via* an energy-dependent endocytic mechanism. Subsequently, the disassembly of VLPs-CaP within lysosomes increased lysosomal membrane permeability, facilitating antigen release into the cytoplasm. Compared to VLPs alone, VLPs-CaP significantly enhanced the activation of DCs. Notably, VLPs-CaP elicited superior humoral as well as cellular immune responses, which are characterized by the increased number of CTLs and enhancing the specific antibody levels (Fig. 1). Therefore, this optimal CaP mineralization offers a valuable technological platform for enhancing the immune and protective effects induced by VLP vaccines.

Experimental

Materials and reagents

$Ca(NO_3)_2{\cdot}4H_2O$ was purchased from Shanghai Hushi Company. $(NH_4)_2HPO_4$ and $NH_4H_2PO_4$ were purchased from Sinopharm. DC2.4 cells were preserved by our laboratory. The ELISA kits for IL-2, IL-12p70, IL-6 and TNF-α were purchased from R&D Company. The lysosomal membrane permeability (LMP)/integrity acridine orange assay kit was purchased from GENMED Company. The Fluo-3 AM calcium ion fluorescent probe was purchased from Beyotime Company. The CellTiter 96 Aqueous One Solution cell proliferation assay was purchased from Promega Company. LPS was purchased from Sigma Company. FITC-anti-CD3, BV421-anti-CD4, APC-cy7-anti-CD8, and other flow cytometry antibodies were purchased from BD Company. Mouse IL-4 (HRP), Mouse IL-2 (HRP), and Mouse IFN-γ (HRP) were purchased from Mabtech Company. Nocodazole, methyl-β-cyclodextrin, and chlorpromazine hydrochloride were purchased from Solarbio. Cytochalasin D was purchased from Aladdin.

Preparation and characterization of FMDV VLPs and VLPs-CaP

Based on the methods previously established in our laboratory, the structural proteins of FMDV were expressed and purified, and then assembled to produce VLPs.[4] The structural proteins were identified by SDS-PAGE and western blot, and the morphology of FMDV VLPs was observed through transmission electron microscopy (TEM). 2 mg of FMDV VLPs was combined with 2 mL of 10 mM $Ca(NO_3)_2$ and stirred at 1500 rpm for 0.5 h at 4 °C. Then, 6 mL of 2 mM $(NH_4)_2HPO_4$/$NH_4H_2PO_4$ was added, followed by stirring at 4 °C (1500 rpm) for 2 h, and the mixture was then allowed to stand for 8 h. The morphology of VLPs-CaP was observed by TEM. The hydrodynamic particle size and zeta potential of FMDV VLPs and VLPs-CaP were determined using dynamic light scattering (DLS). The molecular groups contained in the nanoparticles were characterized by Fourier transform infrared (FT-IR) spectroscopy. The CaP mineralization of FMDV VLPs was identified using SDS-PAGE and western blot. The level of CaP mineralization of FMDV VLPs was determined using the BCA protein assay kit.

Cell uptake levels and mechanisms

Bone marrow-derived dendritic cells (BMDCs) were incubated with FMDV VLPs (10 μg) and VLPs-CaP (containing 10 μg FMDV VLPs) for various time periods (0 h, 1 h, 2 h, 4 h, and 6 h). The uptake of FMDV VLPs and VLPs-CaP by BMDC was

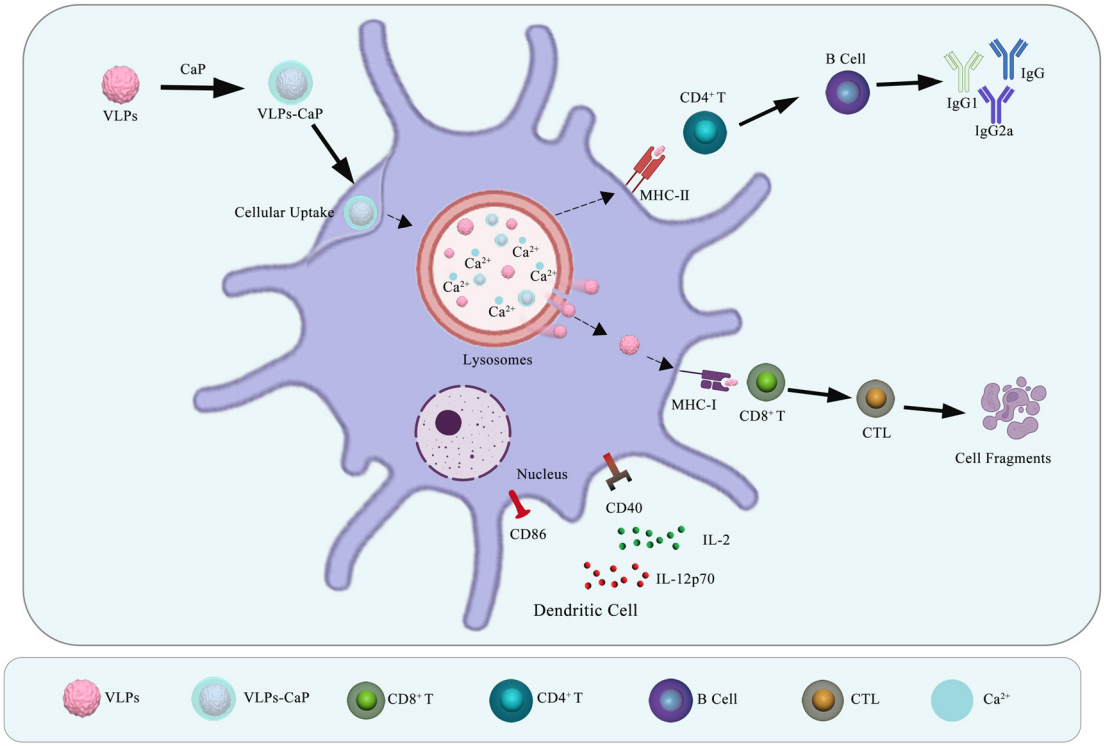

Fig. 1 Schematic representation of the research. VLPs-CaP could effectively activate dendritic cells and enable VLPs to escape into the cytoplasm by increasing the permeability of the lysosomal membrane, consequently inducing potent cellular and humoral immune responses. The material of the figure is sourced from bioGDP.com.[24]

detected using western blot. Subsequently, an indirect immunofluorescence assay was performed, and confocal laser scanning microscopy (CLSM) was utilized to observe the levels of FMDV VLPs in BMDCs after incubation with FMDV VLPs or VLPs-CaP for 6 h. Furthermore, FMDV VLPs were labeled with FITC to prepare VLPs-FITC-CaP nanoparticles. DC2.4 cells were incubated for 1 h with PBS, chlorpromazine hydrochloride (CH) (70 μg mL^{-1}), methyl-β-cyclodextrin (MβC) (120 μg mL^{-1}), cytochalasin D (CD) (100 μg mL^{-1}), or nocodazole (NCDZ) (70 μg mL^{-1}), respectively. The culture medium was discarded, and fresh medium containing VLPs-FITC-CaP (10 μg of FMDV VLPs) was added to DC2.4 cells and incubated for 1 h. Subsequently, the percentage of cells containing VLPs-FITC was determined using flow cytometry. Additionally, VLPs-FITC-CaP were incubated with DC2.4 cells at 4 °C to analyze the energy dependence of cellular uptake.

Antigen-presenting cell activation

Mouse bone marrow-derived macrophages (BMDMs) and BMDCs were seeded into 12-well plates at a density of 5×10^5 cells per mL. Both types of cells were incubated with PBS, FMDV VLPs (10 μg), VLPs-CaP (containing 10 μg of FMDV VLPs), or LPS (10 μg) for 12 h. The cell supernatants were collected, and ELISA was used to detect the levels of cytokines secreted by BMDCs (IL-12p70 and IL-2) and BMDM (IL-6 and TNF-α). The cells were washed three times with PBS. Subsequently, different flow cytometry antibodies were used to stain BMDCs (PE-anti-CD11c, FITC-anti-CD40 and PE-Cy7-anti-CD86). Finally, the activation levels of BMDCs were detected by flow cytometry.

Lysosomal escape level

DC2.4 cells were incubated with VLPs-CaP for various times (0 h, 3 h, and 6 h). After washing three times with PBS, fresh medium containing the 5 μM Fluo-3 AM probe was added, and the cells were further incubated for 40 min. After being washed three times with PBS, the DC2.4 cells were further incubated at 37 °C for 40 min. Intracellular Ca^{2+} levels were detected using CLSM and flow cytometry. Furthermore, DC2.4 cells were incubated with PBS, FMDV VLPs, and VLPs-CaP for 6 h. The lysosomal membrane permeability of cells in different incubation groups was measured using the lysosomal membrane permeability (LMP)/integrity acridine orange assay kit. Then, DC2.4 cells were incubated with FMDV VLPs (10 μg) and VLPs-CaP (containing 10 μg of FMDV VLPs) for 6 h. After being washed three times with PBS, the cells were stained with LysoTracker Red for 0.5 h in the dark. Subsequently, indirect immunofluorescence staining was performed, and the level of antigen and lysosome co-localization was observed through CLSM. Finally, DC2.4 cells were treated with PBS and VLPs-CaP. After incubation for 6 h, lysosensor green DND (LGD) was added to the cells to specifically label lysosomes, with untreated cells without exposure to LGD being used as the control. After incubation for 30 min, flow cytometry and laser

confocal microscopy were used to detect the levels of green fluorescence in the cells.

Mouse immunization

The mouse-related experiments were conducted in strict adherence to the Guidelines for the Care and Use of Laboratory Animals, ensuring the welfare and ethical treatment of the animals. The study was meticulously reviewed and approved by the Animal Ethics Committee of the Lanzhou Veterinary Research Institute, Chinese Academy of Agricultural Sciences, as evidenced by the approval number LVRIAEC-2023-097.

Fifteen female Balb/c mice were randomly divided into three groups and immunized *via* intramuscular injection with PBS, FMDV VLPs, and VLPs-CaP, respectively. Blood samples were collected on days 7, 14, 21 and 28 after immunization. The titers of specific antibodies in the sera were detected using liquid-phase blocking ELISA. The levels of IgG1 and IgG2a in the sera 28 d post-immunization were measured by indirect ELISA. 28 d after immunization, the spleens of the mice were collected, and lymphocyte suspension was obtained using lymphocyte separation medium. The spleen lymphocyte was added to the ELISPOT plate at a density of 3×10^5 cells per well, followed by stimulation with 10 μg mL^{-1} FMDV VLPs for 18 h. The phytohemagglutinin (PHA) incubation group was used as the positive control, and the group without cells was used as the blank control. The spot numbers of IL-2, IFN-γ, and IL-4 were analyzed using a plate reader. A portion of the lymphocytes was added to a 96-well plate at a concentration of 2×10^6 cells per well and incubated with FMDV VLPs for 1 h. Lymphocytes were treated with Brefeldin A (BFA) and incubated for 6 to 8 h. The levels of CTL cells (FITC-anti-CD3, APC-Cy7-anti-CD8, and APC-anti-granzyme B) were analyzed using flow cytometry. Finally, lymphocytes were added to 96-well plates at a concentration of 1×10^6 cells per well to analyze the levels of memory T cells. This involved the use of fluorescently labeled antibodies specific for memory T cell markers, including FITC anti-CD3, BV421-anti-CD4, APC-anti-CD44, and Per-cy5.5-anti-CD62L to identify and quantify these cells using flow cytometry, and memory B cells (FITC anti-CD3, BV500-anti-B220, PE-cy7-anti-IgM and PE-anti-IgD) were analyzed using flow cytometry.

Histological changes

The main organs (heart, liver, spleen, lungs and kidneys) of the mice in different immunization groups (PBS group, FMDV VLPs group and VLPs-CaP group) were collected and fixed in 4% paraformaldehyde solution. The histological changes in the main organs were observed through hematoxylin and eosin (H&E) staining.

Statistical analysis

All data were analyzed using one-way analysis of variance (ANOVA). A level of $P \leq 0.05$ (*) was considered statistically significant.

Results and discussion

Synthesis and characterization of VLPs-CaP

First, FMDV VLPs were prepared according to the protocols established in the laboratory (Fig. 2A and Fig. S1†), by utilizing the ability of Ca^{2+} to bind with carboxyl, hydroxyl, and carbonyl groups present on protein surfaces.[15] Based on previous research,[25] the mineralization conditions were optimized to prepare nanoscale particles of FMDV VLPs-CaP. TEM observations revealed that VLPs-CaP exhibited poor transparency without staining, indicating the presence of the dense mineralized coating (Fig. 2B). The hydrodynamic particle sizes of FMDV VLPs and VLPs-CaP were found to be 43.8 nm and 68.0 nm, respectively, *via* dynamic light scattering (DLS) analysis, indicating that the approximate thickness of the mineralized layer was approximately 12 nm (Fig. 2C). The isoelectric point of CaP was 5.5, indicating a negative charge under physiological pH conditions.[26] DLS measurements indicated that the zeta potential of VLPs-CaP was approximately −6.2 mV (Fig. 2D). FT-IR spectroscopy revealed specific absorption peaks of PO_4^{3-}, Ca^{2+}, and protein groups (–OH, –C═O, –COOR) in the mineralized particles (Fig. 2E), indicating the formation of a CaP mineralization layer on the surface of VLPs. To analyze the level of CaP mineralization of FMDV VLPs, the mineralized sediment and mineralized supernatant were identified by SDS-PAGE and western blot, which showed that the majority of FMDV VLPs were encapsulated by CaP (Fig. 2F). The results of the BCA protein assay revealed that the level of CaP-mineralized FMDV VLPs was about 86.2% (Fig. S2†).

Biocompatibility and uptake mechanism of VLPs-CaP

Good biocompatibility is an essential prerequisite for the use of vaccines.[26] The cytotoxicity assay demonstrated that the viability rate of DC2.4 cells remained above 90% when exposed to VLPs-CaP concentrations up to 100 μg mL^{-1} (Fig. S3A†). Additionally, hemolysis with red blood cells indicated that VLPs-CaP did not cause significant hemolysis at concentrations ranging from 25 μg mL^{-1} to 1000 μg mL^{-1} (Fig. S3B†). These results demonstrated that VLPs-CaP exhibited good biocompatibility. The extent of antigen uptake by DCs is closely related to the efficacy of vaccines in inducing immune responses. The results of western blot (Fig. 3A) and IFA (Fig. 3B) indicated higher antigen content in BMDCs incubated with VLPs-CaP than those treated with FMDV VLPs, suggesting the VLPs-CaP likely facilitates the a more robust and effective immune response.

To clarify the mechanism by which VLPs-CaP were internalized by APCs, flow cytometry was employed to assess the levels of VLPs-CaP uptake following the inhibition of specific endocytic pathways. The inhibitors used included methyl-β-cyclodextrin (MβC) for the caveolar-mediated pathway, cytochalasin D (CD) for the actin-mediated pathway, nocodazole (NCDZ) for the microtubules-mediated pathway and chlorpromazine (CH) for the clathrin-mediated pathway.[27–29] The results showed that the internalization levels of VLPs-CaP

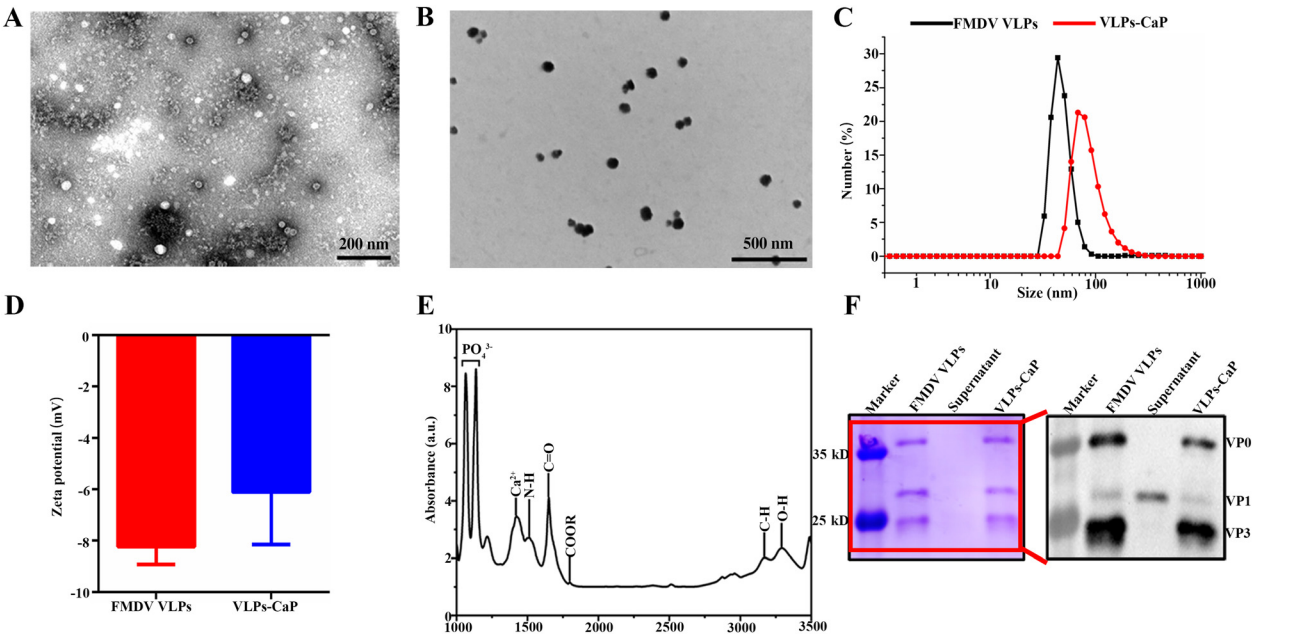

Fig. 2 Characterization of VLPs-CaP. The morphology and size of (A) FMDV VLPs and (B) VLPs-CaP as elucidated by TEM. (C) The hydrodynamic particle size and (D) zeta potential of FMDV VLPs and VLPs-CaP as detected by DLS. (E) FT-IR spectroscopy used to determine the molecular functional groups in VLPs-CaP. (F) The level of FMDV VLPs mineralized by CaP as measured by SDS-PAGE and western blot.

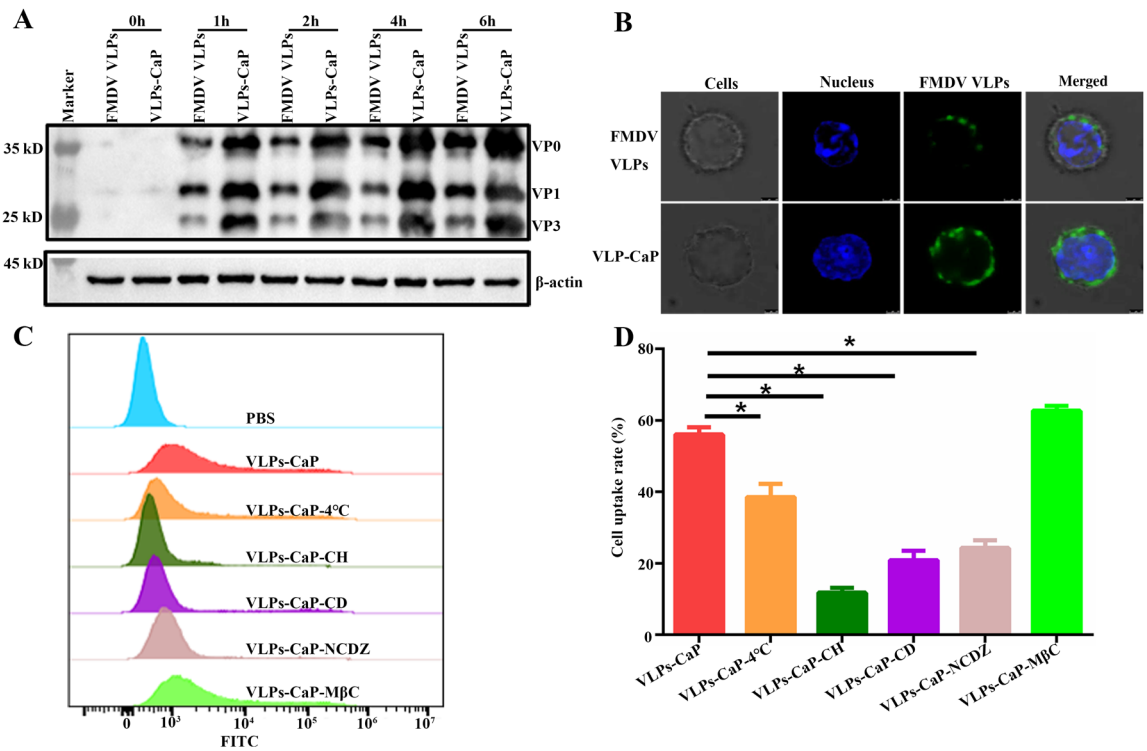

Fig. 3 Cellular uptake levels and mechanism. (A) The levels of FMDV VLPs and VLPs-CaP uptake by BMDCs as assessed using western blot; (B) the intracellular antigen content in BMDCs as visualized using laser confocal microscopy after 6 h of incubation with VLPs-CaP and FMDV VLPs, respectively, to elucidate the antigen distribution within the cells. (C) The uptake levels of VLPs-FITC-CaP by DC2.4 cells after being treated with various inhibitors as measured using flow cytometry; (D) statistical analysis of the flow cytometry results.

was unaffected by MβC. However, marked decreases in uptake were observed: 2.8-fold reduction with cytochalasin D (CD), 2.3-fold reduction with nocodazole (NCDZ), and 4.73-fold reduction with chlorpromazine (CH). These findings suggest that the internalization of VLPs-CaP is mediated through actin, microtubules, and clathrin-dependent endocytosis pathways. Furthermore, incubating cells at 4 °C resulted in a 1.45-fold decrease in the internalization of VLPs-CaP, indicating that the uptake process is energy-dependent (Fig. 3C and D).

APCs activation

APCs function as bridges for antigens to induce specific adaptive immune responses. Once internalized by APCs, the nanovaccine can trigger the maturation of APCs, which leads to an upregulation of the expression level of co-stimulatory molecules.[30,31] Flow cytometry analysis revealed that the levels of CD40 (Fig. 4A) and CD86 (Fig. 4B) of BMDCs incubated with VLPs-CaP were significantly higher than those incubated with FMDV VLPs. Importantly, the levels of IL-2 (Fig. 4C) and IL-12p70 (Fig. 4D) secreted by BMDCs in the VLPs-CaP incubation group were significantly higher than those in the FMDV VLPs group.

As a growth factor capable of driving the expansion of activated T cell populations, IL-2 regulates TH1 cell differentiation as well as the effector and memory responses of $CD8^+$ T cells.[32] IL-12p70 plays a significant role in facilitating the activation of CTLs.[33–35] The synergistic interplay between antigen-activated APCs and cytokines is pivotal in driving the activation of T lymphocytes. These results implied that the CaP-mineralized layer could help VLPs activate DCs and assist in the activation of CTL. Meanwhile, we also discovered that VLPs-CaP could effectively activate BMDMs (Fig. S4†). The aforementioned results demonstrated that CaP mineralization significantly enhanced APCs activation by FMDV VLPs.

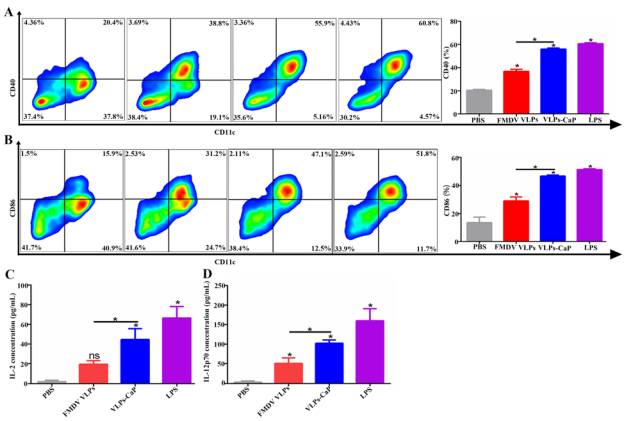

Fig. 4 DC activation level. The expression levels of (A) CD40 and (B) CD86 in BMDCs in different incubation groups (PBS, FMDV VLPs, VLPs-CaP and LPS) as measured by flow cytometry; the secretion levels of (C) IL-2 and (D) IL-12p70 by BMDCs in different incubation groups as detected by ELISA.

Lysosomal escape

To explore the mechanism by which CaP mineralization promotes the immune response, we conducted a series of experiments. CLSM and flow cytometry analyses revealed that Ca^{2+} levels in DC2.4 cells gradually increased with the prolonged incubation time of VLPs-CaP, suggesting that VLPs-CaP decomposed and released large amounts of Ca^{2+} after entering the cells (Fig. 5A, B and Fig. S5†). To delineate whether intracellular Ca^{2+} elevation in DC2.4 cells following VLPs-CaP incubation originates from CaP dissolution, extracellular uptake, or endoplasmic reticulum (ER) release, we cultured the cells in Ca^{2+}-free medium and pharmacologically inhibited ER Ca^{2+} release pathways to assess their respective contributions. The results showed that after VLPs-CaP incubation, the average fluorescence intensity of DC2.4 cells in the Ca^{2+}-free culture medium (VLPs-CaP-CF) group or the Ruthenium Red blocker (cells in the Ca^{2+}-free culture medium) (VLPs-CaP-CF-R) group was lower than that in the VLPs-CaP-cultured DC2.4 cells, but there was no significant difference. Moreover, the mean fluorescence intensity in DC2.4 cells of the VLPs-CaP-CF group and VLPs-CaP-CF-R group was higher than that in the PBS-incubated DC2.4 cells (Fig. S6†). This suggests that while the cytosolic Ca^{2+} flux induced by VLPs-CaP is influenced by extracellular Ca^{2+} influx and endoplasmic reticulum Ca^{2+} release, it predominantly originates from CaP decomposition and its resulting effects. Notably, the results obtained from the multifunctional microplate reader indicated that the lysosomal permeability of DC2.4 cells incubated with VLPs-CaP was significantly higher than that of those cells treated with VLPs (Fig. 5C), suggesting that the CaP decomposition within the lysosome enhanced the lysosomal permeability. Consequently, intracellular Ca^{2+} mobilization in DC2.4 cells post incubation with VLPs-CaP is mediated through biomineral dissolution and its cascade effects, such as the proton sponge effect.[23]

The elimination of pathogen-infected cells mainly relies on the cytotoxic T lymphocytes (CTL).[36,37] Nevertheless, exogenous antigens are mainly degraded into short peptides within lysosomes and presented to $CD4^+$ T lymphocytes *via* the MHC II molecule.[38] Studies have found that the escape of antigens from the endosome-lysosome into the cytoplasm can be presented by the MHC I molecule, thereby leading to the activation of $CD8^+$ T lymphocytes.[39] Observation using CLSM showed that the colocalization level of antigens with lysosomes in DC2.4 cells incubated with VLPs-CaP was extremely low, while the VLPs exhibited a higher level of co-localization with lysosomes (Fig. 5D). Analysis using Image J showed that approximately 66% of FMDV VLPs in the VLPs-CaP group escaped from the lysosomes into the cytoplasm. This indicates that CaP mineralization enables VLPs to escape from lysosomes into the cytoplasm, which is conducive to the activation of $CD8^+$ T lymphocytes by VLPs.

Research indicates that exogenous antigens can escape into the cytoplasm through three mechanisms: receptor-mediated escape, non-receptor-mediated escape, and nanocarrier-mediated escape.[40–42] Modifying the properties of nanocarriers

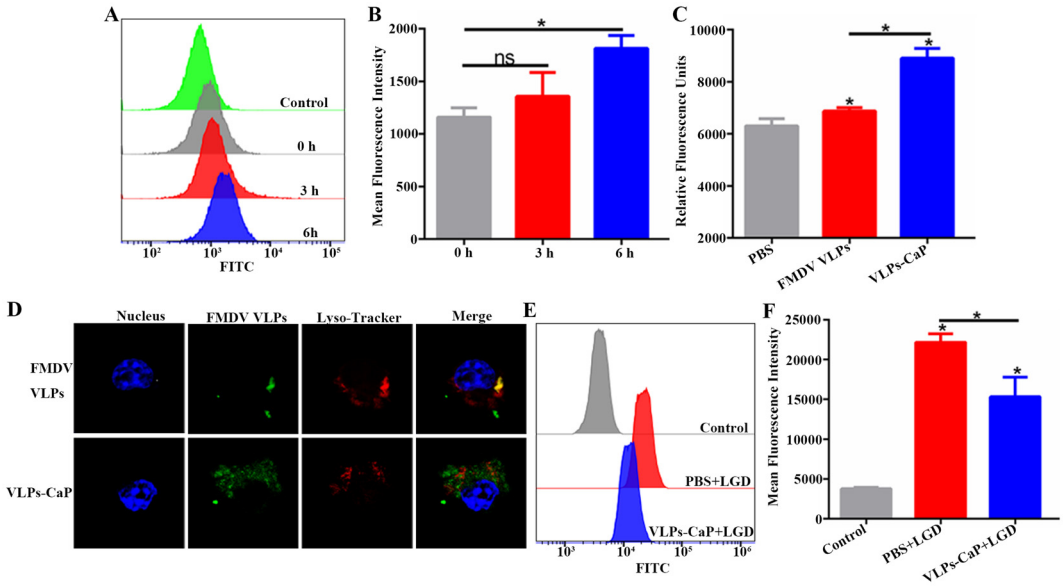

Fig. 5 Lysosomal escape level. (A) Ca^{2+} levels in DC2.4 cells incubated with VLPs-CaP at different time points (0 h, 3 h, and 6 h) as measured using flow cytometry; (B) the mean fluorescence intensity of DC2.4 cells incubated with VLPs-CaP for different periods (0 h, 3 h, and 6 h) as analyzed by FlowJo; (C) lysosomal permeability of DC2.4 cells in different incubation groups (PBS, FMDV VLPs, and VLPs-CaP) as measured using a multifunctional microplate reader; (D) the co-localization level of antigens and lysosomes observed by CLSM after DC2.4 cells were incubated with FMDV VLPs or VLPs-CaP; (E) the fluorescence level in DC2.4 cells of control group (no addition of lysosensor green DND-189(LGD)), PBS-LGD group and VLPs-CaP-LGD group as detected using flow cytometry; (F) analytical results of the mean fluorescence intensity as detected by FlowJo.

can enhance their nanocarrier-mediated escape by promoting degradation within lysosomes. Subsequently, the permeability of the lysosomal membrane increases through the proton sponge effect, promoting the escape of antigens into the cytoplasm.[43,44] To analyze whether VLPs-CaP enhance lysosomal permeability through the proton sponge effect, the lysosensor green DND-189 (LGD) probe, which exhibits fluorescence specifically in acidic organelles such as lysosomes, was employed to assess the changes in lysosomal pH of DC2.4 cells following incubation with VLPs-CaP. The results of flow cytometry (Fig. 5E and F) and laser confocal microscopy (Fig. S7†) showed that the green fluorescence intensity in the cells of the VLPs-CaP group was lower than that of the PBS group. These results indicated that the pH of the lysosomes in the cells of the VLPs-CaP incubation group increased, which suggested that VLPs-CaP may induce the proton sponge effect.

Immune response

The results of *in vitro* experiments suggest that the CaP-mineralized layer has the potential to enhance the cellular immune response of the FMDV VLPs vaccine. To further validate these observations, a murine immunization study was performed, with biological specimens systematically collected at predefined time intervals post-vaccination (Fig. 6A). The RT-qPCR detection of cytokines and chemokines at the injection site showed that the levels of CCL2, CCL3, CCL4, CXCL2, CXCL5, IFN-α, IFN-β, and IL-6 were higher in the VLPs-CaP immunization group compared to those of the FMDV VLPs group (Fig. 6B). These results indicate that the CaP-mineralized layer had the effect of promoting the aggregation of APCs at the injection site and enhancing the activation of APCs. Furthermore, to assess the levels of T lymphocytes in the lymph nodes of vaccinated mice, the levels of $CD4^+$ T cells and $CD8^+$ T cells in the inguinal lymph nodes of mice in different immunization groups (PBS group, FMDV VLPs group, and VLPs-CaP group) were further determined by immunohistochemical analysis. The levels of $CD4^+$ T cells and $CD8^+$ T cells in both the FMDV VLPs immunization group and the VLPs-CaP immunization group were higher than those in the PBS immunization group. Furthermore, CaP mineralization enhanced the level of $CD4^+$ T and $CD8^+$ T cells induced by FMDV VLPs, especially (Fig. S8†). The level of antibodies is one of the important indicators for evaluating the efficacy of vaccines. The level of IgG can reflect the humoral immune response induced by the vaccine. Moreover, IgG1 is associated with the Th2-type of immune response that assists the humoral immune response, while IgG2a is related to the Th1-type of immune response that aids the cellular immune response.[45,46] The antibody level in the sera of immunized mice was measured using ELISA. The results showed that the level of total IgG (Fig. 6C), IgG1 (Fig. S9A†), and IgG2a (Fig. S9B†) was all significantly higher in the VLPs-CaP group than in the FMDV VLPs group. Interestingly, the IgG2a/IgG1 ratio of the VLPs-CaP immunization group was significantly higher than that of the FMDV VLPs immunization group, suggesting that VLPs-CaP induced a more robust Th1-type immune response (Fig. 6D). $CD4^+$ T cells activated by APCs differentiate into various effector cells that assist cellular and

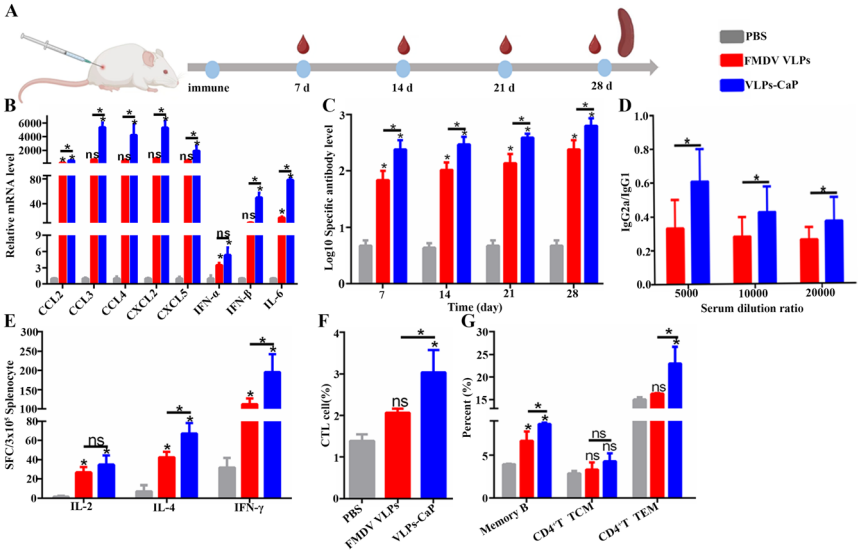

Fig. 6 The level of mouse immune response. (A) Mouse immunization and sample collection procedures; (B) the mRNA levels of chemokines (CCL2, CCL3, CCL4, CXCL2 and CXCL5) and cytokines (IFN-α, IFN-β and IL-6) at the injection sites of mice in different immunization groups (PBS, FMDV VLPs and VLPs-CaP) as detected using RT-qPCR; (C) the levels of specific antibodies in the serum of mice in different immunization groups as detected using liquid-phase blocking ELISA; (D) the ratio of IgG2a/IgG1 in the FMDV VLPs and VLPs-CaP immunization groups; (E) the numbers of splenic lymphocytes secreting IL-2, IL-4 and IFN-γ in the spleen lymphocytes of mice in different immunization groups as detected using ELISPOT; (F) the level of CTL cells in the spleen lymphocytes of mice in different immunization groups as detected by flow cytometry; (G) the levels of memory B cells, CD4+ TCM and CD4$^+$ TEM in the splenic lymphocytes of mice in each immunization group as detected using flow cytometry.

humoral immune responses. Among them, Th1 cells secreting IFN-γ and IL-2 can facilitate the differentiation of CD8$^+$ T cells into CTLs,[47] while Th2 cells secreting IL-4 promote the proliferation and differentiation of B cells and the secretion of antibodies.[48,49] ELISPOT analysis demonstrated that the number of IFN-γ-, IL-2- and IL-4-secreting splenic lymphocytes in the VLPs-CaP immunization group was higher than that in the FMDV VLPs group (Fig. 6E). This suggested that the incorporation of the CaP-mineralized layer augments the induction of both Th1 and Th2 cells by the FMDV VLP vaccine. After being stimulated by antigens, CD8$^+$ T cells differentiate into CTLs, which play a crucial role in cellular immune responses by killing infected cells and blocking the proliferation of pathogens in the body.[50,51] Flow cytometry analysis indicated a significantly higher count of CTLs in the VLPs-CaP group compared to the FMDV VLPs group (Fig. 6F and Fig. S10†), which

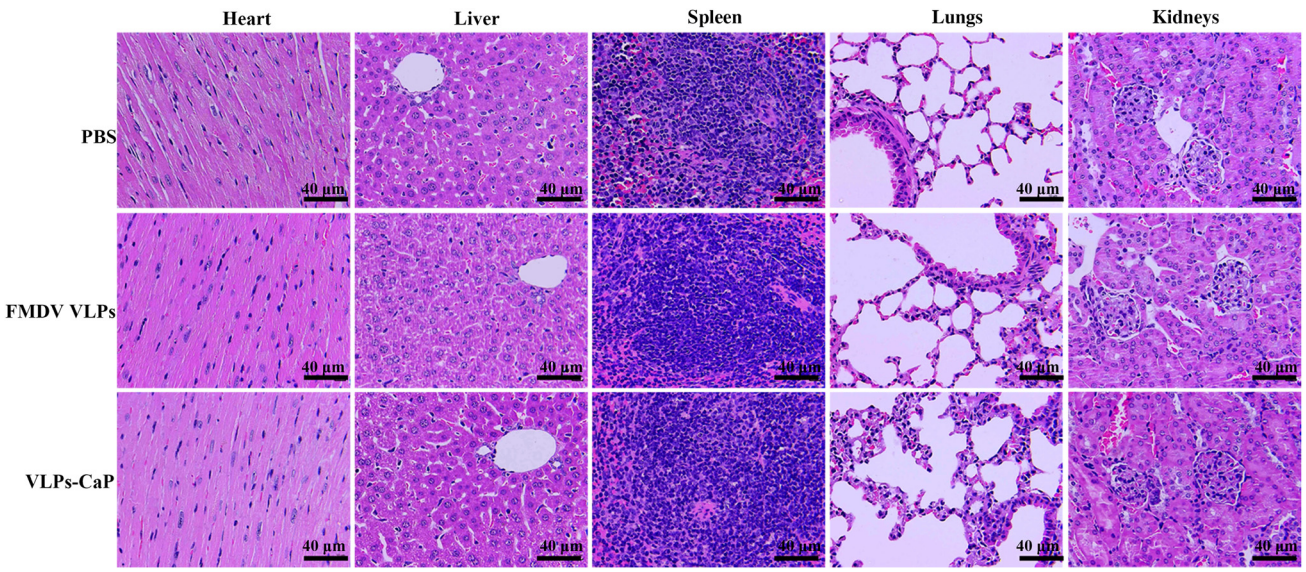

Fig. 7 H&E staining images of the major organs in mice from different immunization groups.

further confirmed that the CaP mineralization layer enhanced cellular immune responses. Together, these results indicated that the VLPs-CaP nanovaccine induced a high level of cellular and humoral immunity.

One of the goals of vaccination is to induce long-lasting immune responses to ensure that the host maintains specific and enduring immune protection against pathogen infection. The duration of vaccine-induced immunity is highly correlated with the abundance of memory immune cells.[52–54] The result of flow cytometry demonstrated that the levels of memory B lymphocytes, $CD4^+$ TEM, and $CD4^+$ TCM in the VLPs-CaP immunization group were all higher than those in the FMDV VLPs group (Fig. 6G, Fig. S11 and S12†). The above results indicated that the CaP-mineralized layer had the effect of enhancing the memory immune response induced by the FMDV VLPs vaccines.

Morphological changes of organs measured by H&E staining

Prerequisites for the application of vaccines are their good biocompatibility and inability to cause severe side effects in vaccinated individuals. Morphological changes of the major organs (heart, liver, spleen, lungs and kidneys) of mice in different immunization groups were observed through H&E staining. It was found that compared with the PBS group, there were no significant pathological changes in the organs of the FMDV VLPs group and the VLPs-CaP group (Fig. 7). Therefore, the CaP mineralization layer did not cause damage to the vaccinated individuals. This may be attributed to the fact that CaP is a component of bones and teeth and is easily absorbed by the body.[21]

Conclusions

In conclusion, the mechanisms underlying the enhanced immune responses induced by CaP-mineralized VLPs was comprehensively investigated. VLPs-CaP was internalized by DCs through an energy-dependent endocytic pathway. Subsequently, the VLPs-CaP nanovaccine was decomposed within lysosomes, which increased the permeability of the lysosomal membrane, facilitating the escape of FMDV VLPs into the cytoplasm. Thus, CaP mineralization elevated the ability of FMDV VLPs to activate DCs and promoted the secretion of Th1-type cytokines. The immune response in mice further clarifies that CaP mineralization could enhance the Th1 immune response and the level of CTLs induced by the FMDV VLPs. Additionally, CaP mineralization also promoted the humoral immunity and memory immunity induced by the FMDV VLPs. Consequently, the VLPs-CaP nanovaccines could induce a high level of coordinated humoral and cellular immune response, providing a new strategy for advancing the application of VLP vaccines.

Author contributions

The manuscript was written through the contributions of all authors. All authors have approved the final version of the manuscript. Z. T. and J. L. contributed equally to this work and should be regarded as co-first authors.

Data availability

The data supporting this article have been included as part of the ESI.†

Conflicts of interest

No potential conflict of interest was reported by the author(s).

Acknowledgements

This work was supported by the National Natural Science Foundation of China (32473012, 32301127), The Major Science and Technology Project of Gansu Province (24ZDWA004), Key R&D Program of Ningxia province (2024BBF02017), Technology innovation guidance program of Gansu Province (24CXNA030), Natural Science Foundation of Gansu Province (23JRRA551, 24JRRA012), and China Postdoctoral Science Foundation Funded Project (2023M733819). We also thank the support of Lanzhou Veterinary Research Institute in the animal house for facilitating the active development of animal experiments. The authors would like to thank Mrs Shuyun Qi, Mrs Yanhong Liu and Mrs Zhenli Gong for their help in the use of experimental equipment.

References

1 K. M. Frietze, D. S. Peabody and B. Chackerian, *Curr. Opin. Virol.*, 2016, **18**, 44–49.
2 J. Fuenmayor, F. Gòdia and L. Cervera, *New Biotechnol.*, 2017, **39**, 174–180.
3 M. O. Mohsen, L. Zha, G. Cabral-Miranda and M. F. Bachmann, *Semin. Immunol.*, 2017, **34**, 123–132.
4 H. C. Guo, S. Q. Sun, Y. Jin, S. L. Yang, Y. Q. Wei, D. H. Sun, S. H. Yin, J. W. Ma, Z. X. Liu, J. H. Guo, J. X. Luo, H. Yin, X. T. Liu and D. X. Liu, *Vet Res*, 2013, **44**, 48.
5 Y. Xiao, S. Zhang, H. Yan, X. Geng, Y. Wang, X. Xu, M. Wang, H. Zhang, B. Huang, W. Pang, M. Yang and K. Tian, *Front. Vet. Sci.*, 2021, **8**, 633706.
6 M. Li, Z. Liang, C. Chen, G. Yu, Z. Yao, Y. Guo, L. Zhang, H. Bao, D. Fu, X. Yang, H. Wang, C. Xue and B. Sun, *ACS Nano*, 2022, **16**, 10482–10495.
7 U. Karakus, M. Sempere Borau, P. Martínez-Barragán, J. von Kempis, S. Yildiz, L. M. Arroyo-Fernández, M. O. Pohl, J. A. Steiger, I. Glas, A. Hunziker, A. García-Sastre and S. Stertz, *Nat. Microbiol.*, 2024, **9**, 2626–2641.
8 I. J. Amanna and M. K. Slifka, *Virology*, 2011, **411**, 206–215.
9 R. A. Seder and A. V. Hill, *Nature*, 2000, **406**, 793–798.

10 Y. Zhou, K. Liu and H. Zhang, *ACS Appl. Bio Mater.*, 2023, **6**, 3516–3531.
11 X. Zeng, Z. Wang, A. Zhao, Y. Wu, Z. Wang, A. Wu, Q. Wang, X. Xia, X. Chen, W. Zhao, B. Li, Z. Lu, Q. Lv, G. Li, Z. Zuo, F. Wu, Y. Zhao, T. Wang, G. Nie, S. Li and G. Zhang, *Nat. Mater.*, 2025, **24**, 287–296.
12 B. Li, Y. Cui, X. Wang and R. Tang, *WIREs Nanomed. Nanobiotechnol.*, 2021, **13**, DOI: **10.1002/wnan.1706**.
13 Z. Wang, L. Wang, N. Prabhakar, Y. Xing, J. M. Rosenholm, J. Zhang and K. Cai, *Acta Biomater.*, 2019, **86**, 416–428.
14 L. Guo, J. Ding and W. Zhou, *Acta Pharm. Sin. B*, 2023, **13**, 5074–5090.
15 D. Chiu, W. Zhou, S. Kitayaporn, D. T. Schwartz, K. Murali-Krishna, T. J. Kavanagh and F. Baneyx, *Bioconjugate Chem.*, 2012, **23**, 610–617.
16 W. Zhou, A. O. Moguche, D. Chiu, K. Murali-Krishna and F. Baneyx, *Nanomedicine*, 2014, **10**, 571–578.
17 R. Su, J. Gu, J. Sun, J. Zang, Y. Zhao, T. Zhang, Y. Chen, G. Chong, W. Yin, X. Zheng, B. Liu, L. Huang, S. Ruan, H. Dong, Y. Li and Y. Li, *J. Nanobiotechnol.*, 2023, **21**, 120.
18 X. Zhong, Y. Zhang, L. Tan, T. Zheng, Y. Hou, X. Hong, G. Du, X. Chen, Y. Zhang and X. Sun, *J. Controlled Release*, 2019, **300**, 81–92.
19 X. Zeng, Z. Wang, A. Zhao, Y. Wu, Z. Wang, A. Wu, Q. Wang, X. Xia, X. Chen, W. Zhao, B. Li, Z. Lu, Q. Lv, G. Li, Z. Zuo, F. Wu, Y. Zhao, T. Wang, G. Nie, S. Li and G. Zhang, *Nat. Mater.*, 2025, **24**, 287–296.
20 P. Spencer, Q. Ye, N. J. B. Kamathewatta, S. K. Woolfolk, B. S. Bohaty, A. Misra and C. Tamerler, *Front. Mater.*, 2021, **8**, DOI: **10.3389/fmats.2021.681415**.
21 Y. Corripio-Miyar, C. L. MacLeod, I. Mair, R. J. Mellanby, B. D. Moore and T. N. McNeilly, *Vaccines*, 2023, **11**, DOI: **10.3390/vaccines11071229**.
22 N. Goto, H. Kato, J. Maeyama, M. Shibano, T. Saito, J. Yamaguchi and S. Yoshihara, *Vaccine*, 1997, **15**, 1364–1371.
23 M. Hayashi, T. Aoshi, Y. Kogai, D. Nomi, Y. Haseda, E. Kuroda, K. Kobiyama and K. J. Ishii, *Vaccine*, 2016, **34**, 306–312.
24 S. Jiang, H. Li, L. Zhang, W. Mu, Y. Zhang, T. Chen, J. Wu, H. Tang, S. Zheng, Y. Liu, Y. Wu, X. Luo, Y. Xie and J. Ren, *Nucleic Acids Res.*, 2025, **53**, D1670–d1676.
25 M. Guo, J. Li, Z. Teng, M. Ren, H. Dong, Y. Zhang, J. Ru, P. Du, S. Sun and H. Guo, *Vaccines*, 2021, **9**, DOI: **10.3390/vaccines9080891**.
26 S. Naahidi, M. Jafari, F. Edalat, K. Raymond, A. Khademhosseini and P. Chen, *J. Controlled Release*, 2013, **166**, 182–194.
27 D. Cai, W. Gao, B. He, W. Dai, H. Zhang, X. Wang, J. Wang, X. Zhang and Q. Zhang, *Biomaterials*, 2014, **35**, 2283–2294.
28 G. Apodaca, *Traffic*, 2001, **2**, 149–159.
29 M. Kaksonen and A. Roux, *Nat. Rev. Mol. Cell Biol.*, 2018, **19**, 313–326.
30 J. Wang, Y. Zhang, Y. Jia, H. Xing, F. Xu, B. Xia, W. Lai, Y. Yuan, X. Li, S. Shan, J. Chen, W. Guo, J. Zhang, A. Zheng, J. Li, N. Gong and X. J. Liang, *Nat. Biomed. Eng.*, 2025, **9**, 201–214.
31 C. Ma, X. Ma, B. Jiang, H. Pan, X. Liao, L. Zhang, W. Li, Y. Luo, Z. Shen, X. Cheng, M. Lian and Z. Wang, *Signal Transduction Targeted Ther.*, 2021, **6**, 353.
32 R. Spolski, P. Li and W. J. Leonard, *Nat. Rev. Immunol.*, 2018, **18**, 648–659.
33 C. S. Garris, S. P. Arlauckas, R. H. Kohler, M. P. Trefny, S. Garren, C. Piot, C. Engblom, C. Pfirschke, M. Siwicki, J. Gungabeesoon, G. J. Freeman, S. E. Warren, S. Ong, E. Browning, C. G. Twitty, R. H. Pierce, M. H. Le, A. P. Algazi, A. I. Daud, S. I. Pai, A. Zippelius, R. Weissleder and M. J. Pittet, *Immunity*, 2022, **55**, 1749.
34 B. C. Gilmour, A. Corthay and I. Øynebråten, *npj Vaccines*, 2024, **9**, 83.
35 A. Zobywalski, M. Javorovic, B. Frankenberger, H. Pohla, E. Kremmer, I. Bigalke and D. J. Schendel, *J. Transl. Med.*, 2007, **5**, 18.
36 M. E. Pipkin, J. A. Sacks, F. Cruz-Guilloty, M. G. Lichtenheld, M. J. Bevan and A. Rao, *Immunity*, 2010, **32**, 79–90.
37 B. J. Johnson, E. O. Costelloe, D. R. Fitzpatrick, J. B. Haanen, T. N. Schumacher, L. E. Brown and A. Kelso, *Proc. Natl. Acad. Sci. U. S. A.*, 2003, **100**, 2657–2662.
38 C. G. Rappazzo, B. D. Huisman and M. E. Birnbaum, *Nat. Commun.*, 2020, **11**, 4414.
39 D. Hirschhorn, S. Budhu, L. Kraehenbuehl, M. Gigoux, D. Schröder, A. Chow, J. M. Ricca, B. Gasmi, O. De Henau, L. M. B. Mangarin, Y. Li, L. Hamadene, A. L. Flamar, H. Choi, C. A. Cortez, C. Liu, A. Holland, S. Schad, I. Schulze, A. Betof Warner, T. J. Hollmann, A. Arora, K. S. Panageas, G. A. Rizzuto, R. Duhen, A. D. Weinberg, C. N. Spencer, D. Ng, X. Y. He, J. Albrengues, D. Redmond, M. Egeblad, J. D. Wolchok and T. Merghoub, *Cell*, 2023, **186**, 1432–1447.
40 M. C. Tan, A. M. Mommaas, J. W. Drijfhout, R. Jordens, J. J. Onderwater, D. Verwoerd, A. A. Mulder, A. N. van der Heiden, D. Scheidegger, L. C. Oomen, T. H. Ottenhoff, A. Tulp, J. J. Neefjes and F. Koning, *Eur. J. Immunol.*, 1997, **27**, 2426–2435.
41 J. D. Colbert, F. M. Cruz and K. L. Rock, *Curr. Opin. Immunol.*, 2020, **64**, 1–8.
42 P. Chen, W. Yang, T. Hong, T. Miyazaki, A. Dirisala, K. Kataoka and H. Cabral, *Biomaterials*, 2022, **288**, 121748.
43 G. Du and X. Sun, *Curr. Opin. Biotechnol*, 2020, **66**, 113–122.
44 Y. Liu, N. Wang, M. Li, Z. Gao, G. Zhang, Y. Yang, S. Wei, J. Hao, J. Cui, Q. Yu and S. Zhai, *Chem. Mater.*, 2024, **36**, 5017–5027.
45 K. M. Toellner, S. A. Luther, D. M. Sze, R. K. Choy, D. R. Taylor, I. C. MacLennan and H. Acha-Orbea, *J. Exp. Med.*, 1998, **187**, 1193–1204.
46 J. Strid, R. Callard and S. Strobel, *Immunology*, 2006, **119**, 27–35.

47 R. V. Luckheeram, R. Zhou, A. D. Verma and B. Xia, *Clin. Dev. Immunol.*, 2012, **2012**, 925135.
48 D. Suzuki, K. Furukawa, F. Kimura, H. Shimizu, H. Yoshidome, M. Ohtsuka, A. Kato, H. Yoshitomi and M. Miyazaki, *Surgery*, 2010, **148**, 573–581.
49 P. Choi and H. Reiser, *Clin. Exp. Immunol.*, 1998, **113**, 317–319.
50 A. Poran, D. Harjanto, M. Malloy, C. M. Arieta, D. A. Rothenberg, D. Lenkala, M. M. van Buuren, T. A. Addona, M. S. Rooney, L. Srinivasan and R. B. Gaynor, *Genome Med.*, 2020, **12**, 70.
51 R. D. Paucek, D. Baltimore and G. Li, *Trends Immunol.*, 2019, **40**, 292–309.
52 M. I. Saeed, A. R. Omar, M. Z. Hussein, I. M. Elkhidir and Z. Sekawi, *Clin. Exp. Vaccine Res.*, 2015, **4**, 88–98.
53 M. K. MacLeod, A. S. McKee, A. David, J. Wang, R. Mason, J. W. Kappler and P. Marrack, *Proc. Natl. Acad. Sci. U. S. A.*, 2011, **108**, 7914–7919.
54 J. Wu, J. Nie, L. Zhang, H. Song, Y. An, Z. Liang, J. Yang, R. Ding, S. Liu, Q. Li, T. Li, Z. Cui, M. Zhang, P. He, Y. Wang, X. Qu, Z. Hu, Q. Wang and W. Huang, *Signal Transduction Targeted Ther.*, 2022, **7**, 18.